Instability of the split-step method for a signal with nonzero central frequency

T.I. Lakoba*

October 18, 2013

Abstract

We obtain analytical conditions for the occurrence of numerical instability of a split-step method (SSM) when the simulated solution of the nonlinear Schrödinger equation is close to a plane wave with nonzero carrier frequency. We also numerically study such an instability when the solution is a sequence of pulses rather than a plane wave. The plane-wave-based analysis gives reasonable predictions for the frequencies of the numerically unstable Fourier modes, but overestimates the instability growth rate. The latter is found to be strongly influenced by the randomness of the signal's profile: the more randomly it varies during the propagation, the weaker is the numerical instability. Using an example of a realistic transmission system, we demonstrate that our single-channel results can be used to predict occurrences of numerical instability in multi-channel simulations. We also give an estimate for the integration step size for which numerical instability, while present, will not affect simulation results for such systems. Using that estimate may lead to a significant saving of computational time.

OCIS codes: (000.4430) Numerical approximation and analysis; (060.4370) Nonlinear optics, fibers; (060.5530) Pulse propagation and temporal solitons.

*Department of Mathematics and Statistics, 16 Colchester Ave., University of Vermont, Burlington, VT 05401, USA (tlakoba@uvm.edu).

1 Introduction

The split-step method (SSM) is widely used in numerical simulations of evolution equations in various areas of physics. In this paper, we focus on a generalized nonlinear Schrödinger equation:

$$iu_z - (\beta_2/2)u_{tt} - i(\beta_3/6)u_{ttt} + \gamma u|u|^2 = 0\,. \tag{1}$$

In fiber optics, u, z, and t are, respectively, the complex envelope of the electric field, the propagation distance along the fiber, and the time in the reference frame moving with the signal. The coefficients $\beta_{2,3}$ are the second- and third-order group-velocity dispersions, and γ is the nonlinear coefficient of the fiber ([1], Sec. 2.3).

The SSM solves Eq. (1) by steps which alternatively account for dispersion and nonlinearity:

$$\begin{array}{l} \text{for } n \text{ from 1 to } n_{\max} \text{ do:} \\ \quad \bar{u}(t) = u_n(t)\,\exp\left[i\gamma|u_n(t)|^2\Delta z\right] \qquad \text{(nonlinear step)} \\ \quad u_{n+1}(t) = \left\{ \begin{array}{l} \text{solution of } \ iu_z = (\beta_2/2)u_{tt} + i(\beta_3/6)u_{ttt} \\ \text{at } z = \Delta z \text{ with initial condition } \bar{u}(t) \end{array} \right. \qquad \text{(dispersive step)} \end{array} \tag{2}$$

where two different implementations of the dispersive step will be discussed below. In (2), Δz is the step of numerical integration and $u_n(t) \equiv u(t, n\Delta z)$.

Scheme (2) yields a numerical solution of (1) whose accuracy is $O(\Delta z)$. Higher-order schemes, yielding more accurate solutions (e.g., with accuracy $O(\Delta z^{\,2})$, $O(\Delta z^{\,4})$, etc.), are well-known [2, 3], but here we will restrict our attention to the lowest-order scheme (2). In fact, all the results obtained below for scheme (2) also hold for the second-order accurate scheme ([2]; [1], Sec. 2.4); for higher-order schemes, they can be obtained in a similar manner. Let us also note that there has been a substantial body of research on controlling the accuracy of the SSM by judiciously choosing the step size Δz; see, e.g., [4, 5] and references therein. However, below we will consider only the case of constant Δz.

In this paper we study the numerical instability (NI) of the SSM when the simulated solution of (1) is approximated by a moving plane wave:

$$u_{\rm pw} = A\,\exp[i\Omega_0 t - iK_0 z], \qquad K_0 = -\big(\beta_2\Omega_0^2/2 - \beta_3\Omega_0^3/6\big), \tag{3}$$

with $\Omega_0 \neq 0$. This solution is a simplest model of a signal propagating with a group velocity $dK_0/d\Omega_0 = -(\beta_2\Omega_0 - \beta_3\Omega_0^2/2)$ relative to some, arbitrarily chosen, reference frame. Given this arbitrariness, one could set $\Omega_0 = 0$ if the signal were the only one

propagating. However, one typically deals with propagation of many channels, and so Ω_0 in this study will denote a carrier frequency of a particular channel.

The plane wave (3) simplifies a realistic signal in that it has a constant amplitude and hence, strictly speaking, carries no information. A realistic signal channel consists of a sequence of pulses. Earlier studies, pertaining to a *single* soliton [6, 7], indicate that a NI of a multi-pulse solution will be different from a NI of the plane wave (3). Nonetheless, we will demonstrate below that some of the characteristics of the NI around a plane wave carry over to the NI around a more realistic, multi-pulse signal. We will also exhibit differences between these two types of NI.

Let us emphasize that the issue of numerical stability of the SSM (or of any numerical method) is *not*, in general, related to the issue of controlling the size of the error at one simulation step (the local error), which has been considered in earlier studies [2]–[5]. (Although for a sufficiently small local error, the SSM is expected to be stable, below we will exhibit a situation where this is not so. That is, in that special case, the numerical error will exponentially grow with the propagation distance — albeit, perhaps, slowly — for any Δz, no matter how small.) Both smallness of the local error and stability are required for the numerical method to produce accurate results; this is the well-known Lax theorem which is often stated in abbreviated form as: 'approximation plus stability imply convergence'. In this paper we do *not* consider the size of the local error of the SSM, but instead focus on the conditions of the method's stability. In fiber optics literature, NI of the SSM is sometimes referred to as "spurious four-wave mixing" (FWM) [8].

We will now discuss two implementations of scheme (2), which differ by their treatment of the dispersive step. In most applications, it is computed by the Fourier spectral method:

$$u_{n+1}(t) = \mathcal{F}^{-1}\left[\exp[iP(\omega)]\ \ \mathcal{F}[\bar{u}(t)]\right], \tag{4}$$

where

$$P(\omega) = (\beta_2\omega^2/2 - \beta_3\omega^3/6)\Delta z. \tag{5}$$

Here $\mathcal{F}$ and $\mathcal{F}^{-1}$ are the discrete Fourier transform and its inverse, and ω is the discrete frequency:

$$-\omega_{\max} \le \omega \le \omega_{\max}, \qquad \omega_{\max} = \pi/\Delta t, \tag{6}$$

where Δt is the mesh size of the computational domain. We will refer to the SSM (2) where the dispersive step is implemented by the spectral method (4) and (5), as the s-SSM.

On the other hand, when $\beta_3 = 0$, the dispersive step in (2) can also be efficiently

computed by a finite-difference method:

$$i\frac{u_{n+1}^m - \bar{u}^m}{\Delta z} = \frac{\beta}{2}\left(\frac{u_{n+1}^{m+1} - 2u_{n+1}^m + u_{n+1}^{m-1}}{\Delta t^{\,2}} + \frac{\bar{u}^{m+1} - 2\bar{u}^m + \bar{u}^{m-1}}{\Delta t^{\,2}}\right), \tag{7}$$

where $u_n^m \equiv u(t_m, n\Delta z)$, $\bar{u}$ is the "intermediate" solution defined in (2), $-T/2 \le t_m < T/2$, and T is the length of the computational domain. We will refer to the SSM (2) where the dispersive step is implemented by the finite-difference method (7), as the fd-SSM. Recently, this and similar methods have found an application in the electronic post-processing of optical signals [9]. That post-processing must be done in real time, and hence the speed of its implementation becomes a key factor. References [10, 11] showed that finite-difference implementations, more sophisticated than (7) (see, e.g., Eqs. (13) and (22) in [10]), may yield a speed-up over the spectral implementation (5) while retaining high accuracy. Also, let us note that the so-called discrete nonlinear Schrödinger equation, where in (1) $\beta_3 = 0$ and the second derivative is replaced by its finite-difference approximation, similarly to (7), is of considerable interest in its own right [12].

We assume that the simulations use periodic boundary conditions:

$$u(-T/2, z) = u(T/2, z). \tag{8}$$

Then (7) can be written as Eq. (4) where now

$$P(\omega) = 2\arctan\left[\beta_2 r \sin^2(\omega\Delta t/2)\right], \qquad r = \Delta z/\Delta t^{\,2}. \tag{9}$$

Expressions (5) and (9) are compared in Fig. 1. It is the difference of these expressions at high values of ω that leads to the NI of the s- and fd-SSMs being qualitatively different, as will be shown below.

NI of both implementations, s- and fd-, of the SSM for Eq. (1) with $\beta_3 = 0$ was first studied in [13], when the simulated solution was close to the *standing* plane wave, Eq. (3) with $\Omega_0 = 0$. It was shown that the s-SSM is conditionally stable for both signs of β_2, while the fd-SSM is conditionally stable for $\beta_2 > 0$ and unconditionally stable for $\beta_2 < 0$. Similar results about the s-SSM have later been obtained in a number of other studies; see, e.g., [14, 15]. Numerical stability of the plane wave solution of the SSM and related methods has also received renewed attention very recently [16, 17].

In Section 2 we will set up the von Neumann stability analysis that applies to both implementations of the SSM, and in Sections 3 and 4 will obtain specific conclusions for the s- and fd-SSMs, respectively. In Section 5 we will carry out numerical simulations with two goals in mind. First, we will simulate propagation of a strongly nonlinear

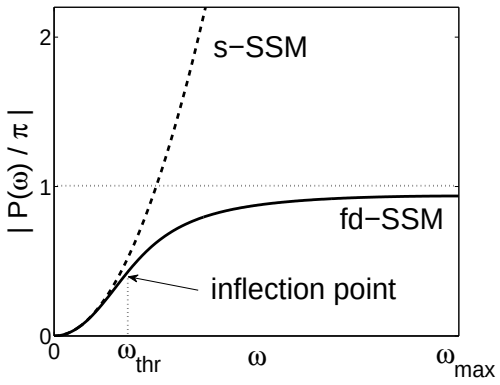

Figure 1: Comparison of expressions (5) and (9).

single channel carrying a multi-pulse signal and exhibit both similarities and differences between the NI of a plane wave and a multi-pulse signal. Second, we will give an example of NI in a realistic (i.e., weakly nonlinear) fiber-optical telecommunication system and demonstrate that the analysis of this paper has predictive power for such a system as well. In Section 6 we will summarize our results and also outline steps that remain to be done to fully understand NI of the SSM in realistic multi-channel systems.

2 Von Neumann analysis of the SSM on a plane-wave background

As with studying NI of any scheme, we assume that the numerical solution u_n of the SSM (2) is close to $u_B = A\exp[i\Omega_0 t + iP(\Omega_0)n]$, which is the numerical approximation of the exact (i.e., in the absence of any round-off error) background solution (3). Here $P(\omega)$ is defined either by (5) or (9). Thus,

$$u_n = u_B + \tilde{u}_n, \qquad |\tilde{u}_n| \ll |u_B|, \tag{10}$$

where $\tilde{u}_n$ is the small numerical error. Substituting (10) into (2) and (4) and linearizing, one obtains:

$$\mathcal{F}\left[\tilde{u}_{n+1}\right] = e^{iP(\omega)}\mathcal{F}\left[e^{i\gamma|u_B|^2\Delta z}\big(\tilde{u}_n + i\gamma\Delta z(u_B^2\tilde{u}_n^* + |u_B|^2\tilde{u}_n)\big)\right]. \tag{11}$$

In what follows we will assume that

$$\Omega_0 > 0 \tag{12}$$

and also that the change of the solution at the nonlinear step of (2) is small:

$$\epsilon \equiv \gamma A^2 \Delta z \ll 1. \tag{13}$$

This condition holds in all practically relevant simulations of (1).

Following [13, 6], we seek $\tilde{u}_n$ in the form:

$$\tilde{u}_n = e^{i\Omega_0 t + iP(\Omega_0)n} \left(p_n\, e^{i\omega_1 t} + q_n^*\, e^{-i\widehat{\omega_1} t} \right). \tag{14}$$

Here, unlike in the previous studies [13, 14, 15, 6], $\widehat{\omega_1}$ must account for aliasing as follows. The frequency of the p-term in (14) is $\Omega_0 + \omega_1 = \omega$, where we assume that $\omega \in [-\omega_{\max}, \omega_{\max})$, and hence $\omega_1 \in [-\omega_{\max} - \Omega_0,\, \omega_{\max} - \Omega_0)$. To make the frequency of the q-term fall within the computational spectrum, we define

$$\Omega_0 - \widehat{\omega_1} = \begin{cases} 2\Omega_0 - \omega & \text{if} \quad 2\Omega_0 - \omega \le \omega_{\max}; \\ 2\Omega_0 - \omega - 2\omega_{\max} & \text{if} \quad 2\Omega_0 - \omega > \omega_{\max}. \end{cases} \tag{15}$$

Substituting (14) into (11) and neglecting terms of order ϵ^2, one obtains a linear recursion relation for the components of the error:

$$\begin{pmatrix} p_{n+1} \\ q_{n+1} \end{pmatrix} = \begin{pmatrix} e^{i\Delta_+}(1 + i\epsilon) & e^{i\Delta_+}\, i\epsilon \\ -e^{i\Delta_-}\, i\epsilon & e^{i\Delta_-}(1 - i\epsilon) \end{pmatrix} \begin{pmatrix} p_n \\ q_n \end{pmatrix}, \tag{16}$$

where

$$\Delta_+ = P(\Omega_0 + \omega_1) - P(\Omega_0), \qquad \Delta_- = P(\Omega_0 - \widehat{\omega_1}) - P(\Omega_0). \tag{17}$$

The eigenvalues of this linear system are:

$$\lambda = \exp\left[i \frac{\Delta_+ - \Delta_-}{2} \right] \left(\frac{\cos(\delta + \epsilon)}{\cos\epsilon} \pm \sqrt{\left(\frac{\cos(\delta + \epsilon)}{\cos\epsilon} \right)^2 - 1} \right), \tag{18}$$

where

$$\delta \equiv \frac{\Delta_+ + \Delta_-}{2} = \frac{1}{2} \left(P(\Omega_0 + \omega_1) - 2P(\Omega_0) + P(\Omega_0 - \widehat{\omega_1}) \right). \tag{19}$$

In deriving (18), we have neglected terms $O(\epsilon^3)$ and hence relpaced $\arctan\epsilon$ with ϵ. NI occurs where $|\lambda| > 1$, which yields

$$N\pi - 2\epsilon < \delta < N\pi, \qquad N \in \mathbb{Z}. \tag{20a}$$

In the next section we will restrict our attention to the case when $P(\omega)$, defined by (5), does not change its sign within the computational spectrum due to $\beta_3 \neq 0$. Then it follows from (5) and (9) that the sign of δ coincides with $\operatorname{sgn}(\beta_2)$. Therefore, in (20a),

$$N = |N| \operatorname{sgn}(\beta_2). \tag{20b}$$

The above derivation has followed the standard lines of [13, 15], except for a minor technical point that those earlier studies did not explicitly use the condition (13). The novelty of (19), (20) compared to the earlier studies is the dependence of δ on Ω_0. In the next two sections we will show what consequences this has to the s- and fd-SSMs.

Before moving on, let us note that (20a) is the condition of *phase-matched* FWM among frequencies $\Omega_0 + \omega_1$, $\Omega_0 - \widehat{\omega_1}$, and Ω_0:

$$P(\Omega_0 + \omega_1) + P(\Omega_0 - \widehat{\omega_1}) - 2P(\Omega_0) \approx 2\pi N. \tag{21}$$

It is for this reason that NI is sometimes referred to "spurious FWM" [8]. In the continuous limit, where $\Delta z \to 0$, (5) and (9) yield $P(\omega) \to 0$, and therefore (21) can only occur for $N = 0$. In that case, the instability is a real physical phenomenon known as modulational instability, which exists only for $(\beta_2 - \beta_3\Omega_0) < 0$ (see, e.g., [1], Sec. 5.1). Numerical, as opposed to real, instability occurs due to $\Delta z \neq 0$, in which case one can have $N \neq 0$ in (21). The above shows that NI is just a form of modulational instability, or, in other words, a particular case of phase-matched FWM. In Section 5 we will distinguish between NI and non-phase-matched FWM and refer to the latter as just FWM.

3 Instability of the s-SSM

For the sake of clarity, we will first consider the case $\beta_3 = 0$ and later on will return to the more general case $\beta_3 \neq 0$.

Substituting (5) and (15) into (19), one finds:

$$\delta = \begin{cases} \beta_2 \Delta z(\omega - \Omega_0)^2/2 \equiv \delta_{\text{main}} & \text{if} \quad \omega \in (-\omega_{\max} + 2\Omega_0,\, \omega_{\max}); \\ \delta_{\text{ali, min}} + \beta_2 \Delta z(\omega - \Omega_0 + \omega_{\max})^2/2 \equiv \delta_{\text{ali}} & \text{if} \quad \omega \in [-\omega_{\max},\, -\omega_{\max} + 2\Omega_0], \end{cases} \tag{22}$$

where

$$\delta_{\text{ali, min}} = \operatorname{sgn}(\beta_2)\pi \frac{\Delta z}{\Delta z_{\text{thr}}}(1 - a^2), \qquad a = \frac{\Omega_0}{\omega_{\max} - \Omega_0}, \tag{23}$$

$$\Delta z_{\text{thr}} = 2\pi / \big(|\beta_2|(\omega_{\max} - \Omega_0)^2\big). \tag{24}$$

We will refer to the first and second frequency intervals in (22) as the "main" and "aliased" intervals, respectively; see Fig. 2(a). The aliased interval contains aliased frequencies, while the main one does not. Sample plots of $\delta(\omega)$ are shown in Fig. 2(b)

for $\beta_2 > 0$; for $\beta_2 < 0$, they are flipped about the horizontal axis. For a reason discussed later in this section, here we will only consider

$$\Omega_0 < 0.5\omega_{\max}. \tag{25}$$

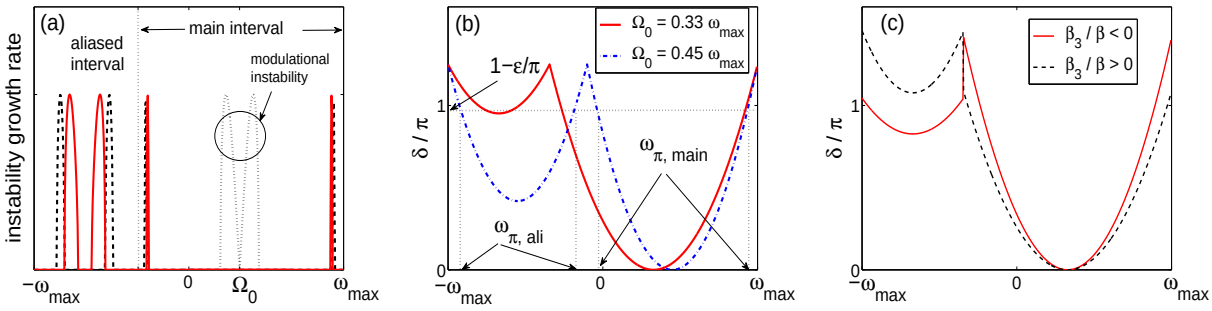

Figure 2: (a) Growth rate of unstable modes for $\Delta z = 1.25\Delta z_{\rm thr}$ and $\Omega_0 = \omega_{\max}/3$: $\beta_2/2 = 1$ (solid red), $\beta_2/2 = -1$ (dashed black); modulationally unstable modes are shown by dotted black line. (b) $\delta(\omega)$ for $\Delta z = 1.25\Delta z_{\rm thr}$, $\beta_2/2 = 1$, $\beta_3 = 0$, and two values of Ω_0; other notations are explained in the text. (c) Similar to (b) with $\Omega_0 = \omega_{\max}/3$, but for $\beta_3 = \pm 0.4\beta_2/\omega_{\max}$. Note that $\delta(\omega)$ is discontinuous. **[NOTES FOR PRODUCTION EDITORS: 1) PLEASE PLACE ALL THREE FIGURES IN ONE ROW (THEY WILL OCCUPY THE WIDTH OF TWO COLUMNS). 2) COLOR ONLINE ONLY.]**

The bands of numerically unstable modes are found from (20) and (22). Their centers are given by:

$$\omega_{N\pi,\,\rm main} = \Omega_0 \pm \sqrt{\frac{|N|\pi - {\rm sgn}\,(\beta_2)\epsilon}{|\beta_2|\Delta z/2}}, \tag{26a}$$

$$\omega_{N\pi,\,\rm ali} = -\omega_{\max} + \Omega_0 \pm \sqrt{\frac{|N|\pi - {\rm sgn}\,(\beta_2)(\delta_{\rm ali,\,min} + \epsilon)}{|\beta_2|\Delta z/2}}, \tag{26b}$$

which exist when the computational step Δz satisfies:

$$\Delta z > \frac{|N|\Delta z_{\rm thr}}{1 + {\rm sgn}\,(\beta_2)\gamma A^2 \Delta z_{\rm thr}/\pi}, \tag{27a}$$

$$\frac{|N|\Delta z_{\rm thr}}{1 + {\rm sgn}\,(\beta_2)\gamma A^2 \Delta z_{\rm thr}/\pi} < \Delta z < \frac{|N|\Delta z_{\rm thr}}{1 - a^2 + {\rm sgn}\,(\beta_2)\gamma A^2 \Delta z_{\rm thr}/\pi}, \tag{27b}$$

respectively. Here $\Delta z_{\rm thr}$ and a have been defined in (24) and (23). An example of the growth rate of these unstable modes, computed as $(|\lambda|-1)/\Delta z$ when $|\lambda|>1$, where λ is given by (18), is shown in Fig. 2(a). At the maxima, all these peaks equal γA^2, as in the $\Omega_0 = 0$ case [15]. Examples of expressions (26) are shown in Fig. 3(a) for $\beta_2 > 0$; for $\beta_2 < 0$, they are very close, as the example shown in Fig. 2(a) illustrates.

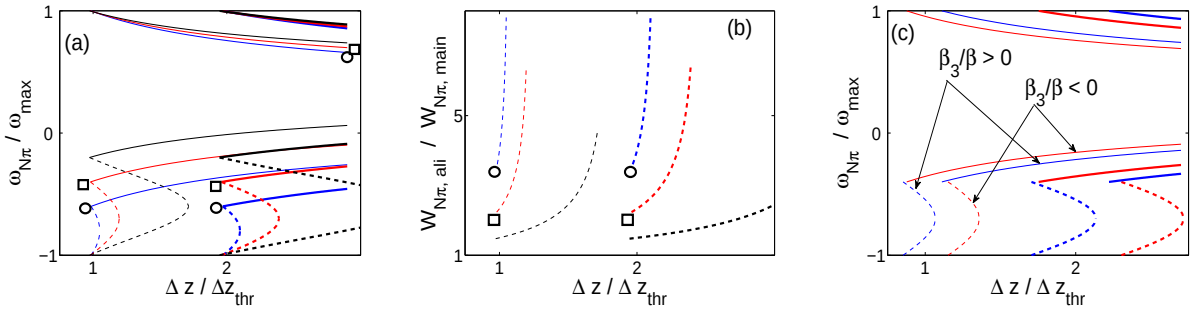

Figure 3: (a) Centers of the instability bands, given by (26), for $\Omega_0/\omega_{\max} = 0.2$ (blue, circle), 0.3 (red, square), and 0.4 (black). Note that $\Delta z_{\rm thr}$ depend on Ω_0. Thin and thick lines are for $N = 1$ and $N = 2$, respectively. Solid and dashed lines are for the instability peaks in the main and aliased intervals, respectively. (b) Ratios of the widths of the same instability bands as in (a). (c) Centers of the instability bands, given by (35), for $\Omega_0/\omega_{\max} = 0.3$ and $\beta_3\omega_{\max}/\beta_2 = -0.4$ (red) and 0.4 (blue). Line thicknesses and styles denote the same as in (a). The pointing arrows emphasize that the curves are discontinuous at $\omega = -\omega_{\max} + 2\Omega_0$. **[NOTES FOR PRODUCTION EDITORS: 1) PLEASE PLACE ALL THREE FIGURES IN ONE ROW (THEY WILL OCCUPY THE WIDTH OF TWO COLUMNS). 2) COLOR ONLINE ONLY.]**

If one neglects the ϵ-term, which is a good approximation in most applications, then Eqs. (26) become:

$$\omega_{N\pi,\,\rm main} \approx \Omega_0 \left[1 \pm \frac{1}{a}\sqrt{|N|\Delta z_{\rm thr}/\Delta z}\right], \tag{28a}$$

$$\omega_{N\pi,\,\rm ali} \approx -(\omega_{\max} - \Omega_0) \left[1 \pm \sqrt{|N|\Delta z_{\rm thr}/\Delta z \; - (1-a^2)}\right], \tag{28b}$$

where we have used (23) and (24). These equations will turn out to be more convenient to use than (26) in Section 5, where we will study dependence of NI on the ratio $\Delta z/\Delta z_{\rm thr}$. Moreover, Eqs. (28) make it apparent that had we included losses and amplification in our model (1), they would not have affected the locations of the NI bands.

Rather, they would have affected their widths (see below) and the instability growth rate.

The widths $W_{N\pi}$ of the NI bands centered at frequencies (26) can be computed from the condition $\delta(\omega_{N\pi} \pm W_{N\pi}/2) = (N\pi - \epsilon) \pm \epsilon$ (see (20)):

$$W_{N\pi,\mathrm{main}} \approx 2\epsilon/\big(|\beta_2|\Delta z\,(\omega_{N\pi,\,\mathrm{main}} - \Omega_0)\big), \qquad N \neq 0; \tag{29a}$$

$$W_{N\pi,\mathrm{ali}} \approx 2\epsilon/\big(|\beta_2|\Delta z\,(\omega_{N\pi,\,\mathrm{ali}} - (-\omega_{\max} + \Omega_0))\big). \tag{29b}$$

The ratio of these widths is shown in Fig. 3(b). In absolute terms, in most cases these widths are rather small so that they accommodate only few nodes of the spectral grid.

The case $N = 0$, explicitly excluded in (29a), corresponds not to a NI, but to the well-known modulational instability, as we noted after (21).

Let us now note that a *numerical* instability corresponding to $N = 0$ in (20) will *always*, i.e., for any step Δz, occur when condition (25) is violated, i.e. when $\Omega_0 > 0.5\omega_{\max}$. This follows from expressions (22) and (23) with $a > 1$. In terms of the situation depicted in Fig. 2(b), this occurs because the curve $\delta_{\mathrm{ali}}(\omega)$ always crosses zero when $\Omega_0 > 0.5\omega_{\max}$; hence the instability condition (20) with $N = 0$ will hold in this case. If one denotes $\Omega_0 = 0.5\omega_{\max}(1 + \mu)$, where $0 < \mu < 1$, then using the same approximation as for (28), one finds spectral locations of this NI:

$$\omega^{\pm}_{\Omega_0 > 0.5\omega_{\max}} = -0.5\omega_{\max}(1 - \mu \pm 2\sqrt{\mu}). \tag{30}$$

Note that they do not depend on either Δz or β_2, but depend only on Ω_0 and $\omega_{\max}$. It is for the reason of avoiding this unconditional NI that we have only considered $\Omega_0 < 0.5\omega_{\max}$ except in the last examples in Sections 5A and 5B. On the other hand, if one allows $\Omega_0 > 0.5\omega_{\max}$, then one can also have additional occurrences of NI for $\Delta z < \Delta z_{\mathrm{thr}}$ when $\delta_{\mathrm{ali,\,min}} = 2\pi L$, with L being a nonzero integer. For example, it follows from (23) that for $\Delta z = 0.8\Delta z_{\mathrm{thr}}$, a new instance of NI will occur at $-(\omega_{\max} - \Omega_0)$ for $\Omega_0 = 0.6\omega_{\max}$. Indeed, $\pi \times 0.8 \times [1 - (0.6/(1 - 0.6))^2] = -2\pi$.

To see how the account for third-order dispersion, β_3, modifies these results, we first note that in most fiber-optical simulations, this term is only a correction to the second-order dispersion term. For example, it is reasonable to assume that the change of the group-velocity dispersion introduced by the β_3-term does not exceed 50% of the group-velocity dispersion at the central frequency, $\omega = 0$, of the simulation domain. This requirement yields:

$$\beta_3\omega_{\max} < 0.5\beta_2, \tag{31}$$

which we will assume in what follows. Most importantly, this requirement means that the group-velocity dispersion will not change its sign anywhere in the computational

domain. Violation of this requirement does not affect the expression in (32) below but makes subsequent formulae more complicated.

The counterpart of Eqs. (22) is:

$$\delta = \begin{cases} (\beta_2 - \beta_3\Omega_0)\,\Delta z(\omega - \Omega_0)^2/2 & \text{if} \quad \omega \in (-\omega_{\max} + 2\Omega_0,\, \omega_{\max}); \\ \delta_{\text{ali, min}} + (\beta_2 + \beta_3(\omega_{\max} - \Omega_0))\,\Delta z(\omega - \Omega_0 + \omega_{\max})^2/2 & \text{if} \quad \omega \in [-\omega_{\max}, -\omega_{\max} + 2\Omega_0], \end{cases} \tag{32}$$

where now

$$\delta_{\text{ali, min}} = \text{sgn}\,(\beta_2)\pi\frac{\Delta z}{\Delta z_{\text{thr}}}\left(1 - a^2 + \frac{\beta_3\omega_{\max}}{3\beta_2}(1 - a + a^2)\right), \tag{33}$$

and Δz_{thr} is still given by (24). Typical plots of (32) are shown in Fig. 2(c). Note that δ is discontinuous at $\omega = -\omega_{\max} + 2\Omega_0$, with the magnitude of the jump being:

$$\delta_{\text{jump}} = \beta_3\Delta z\,\omega_{\max}^3/6. \tag{34}$$

The counterparts of (26) and (27) are, respectively, (35) and (36) below:

$$\omega_{N\pi,\,\text{main}} = \Omega_0 \pm \sqrt{\frac{|N|\pi - \text{sgn}\,(\beta_2)\epsilon}{|\beta_2 - \beta_3\Omega_0|\Delta z/2}}, \tag{35a}$$

$$\omega_{N\pi,\,\text{ali}} = -\omega_{\max} + \Omega_0 \pm \sqrt{\frac{|N|\pi - \text{sgn}\,(\beta_2)(\delta_{\text{ali, min}} + \epsilon)}{|\beta_2 + \beta_3(\omega_{\max} - \Omega_0)|\Delta z/2}}; \tag{35b}$$

$$\Delta z > \frac{|N|\Delta z_{\text{thr}}}{1 - \beta_3\Omega_0/\beta_2 \; + \text{sgn}\,(\beta_2)\gamma A^2\Delta z_{\text{thr}}/\pi}, \tag{36a}$$

$$\frac{|N|\Delta z_{\text{thr}}}{1 - (\beta_3/\beta_2)(\Omega_0 - \omega_{\max}(1 + a)^2/3) \; + \text{sgn}\,(\beta_2)\gamma A^2\Delta z_{\text{thr}}/\pi} <$$

$$\Delta z < \frac{|N|\Delta z_{\text{thr}}}{1 - a^2 + (\beta_3/\beta_2)\omega_{\max}(1 - a + a^2)/3 \; + \text{sgn}\,(\beta_2)\gamma A^2\Delta z_{\text{thr}}/\pi}, \tag{36b}$$

where $\delta_{\text{ali, min}}$ is given by (33). The centers of the NI bands, given by (35), are shown in Fig. 3(c). Counterpart equations of (29) are not explicitly shown here; qualitatively, they are similar to those shown in Fig. 3(b).

4 Instability of the fd-SSM

Recall that in this section, we work with the case $\beta_3 = 0$. We will begin by finding an upper bound, ω_{thr}, for Ω_0, such that for $\Omega_0 > \omega_{\text{thr}}$, the fd-SSM will not be expected to provide even a qualitatively correct solution. The existence of such a bound is clear

from Fig. 1, because for $\omega > \omega_{\rm thr}$, the phase $P(\omega)$, as computed by the finite-difference method (7), changes its concavity. For $\omega > \omega_{\rm thr}$, it no longer captures even the sign of the group-velocity dispersion. Thus, we will restrict our consideration only to $\Omega_0 < \omega_{\rm thr}$ (recall (12)).

The condition $P''(\omega_{\rm thr}) = 0$, which defines $\omega_{\rm thr}$, yields the following equation:

$$x^3 - x + 2 = 4x/(\beta_2 r)^2, \qquad x = \cos(\omega_{\rm thr}\Delta t). \tag{37}$$

To obtain its solution in a useful form, one requires an assumption on the size of $(\beta_2 r)$, which we will now discuss. It is known from [13] that for $\beta_2 > 0$ and $\Omega_0 = 0$, the fd-SSM is stable when Δz is below a threshold value that is on the order of $\Delta t/\sqrt{|\beta_2|\gamma A^2}$ (its exact expression will be given later). (For $\beta_2 < 0$, the fd-SSM is unconditionally stable on the background of a plane wave with $\Omega_0 = 0$; for the stability on the background of a soliton, one also requires $\Delta z < O(\Delta t/\sqrt{|\beta_2|\gamma A^2})$ [7].) Moreover, the fd-SSM may be a viable alternative to the s-SSM only if it is time-efficient, which requires that Δz scale in proportion to Δt rather than to Δt^2. All these considerations suggest that a practical range for Δz is $O(\Delta t/\sqrt{|\beta_2|\gamma A^2})$. Then $|\beta_2| r = \Delta z/\Delta t^2$ is large:

$$|\beta_2| r = O(1/(\gamma A^2 \Delta z)) \equiv 1/\epsilon \gg 1. \tag{38}$$

Under condition (38), a physically relevant solution of (37), $x \approx 1 - 2/(\sqrt{3}\beta_2 r)$, is found by a standard asymptotic method (see, e.g., [18]), which yields:

$$\omega_{\rm thr} \approx 2/(3^{1/4}\sqrt{|\beta_2|\Delta z}). \tag{39}$$

One can also verify that for $|\beta_2| r > 4$, $P''(\omega)$ is within 10% of its nominal value of $\beta_2 \Delta z$ for $|\omega| \le 0.5\omega_{\rm thr}$. Therefore, in what follows we will restrict our consideration to the case

$$\Omega_0 \le 0.5\omega_{\rm thr}. \tag{40}$$

Then (40), (39), and (38) imply that $\Omega_0 \ll \omega_{\max}$ $(= O(\Delta t^{-1}))$. At the end of this section we will illustrate what happens if the condition $\Omega_0 < \omega_{\rm thr}$ is violated.

Now, from the expression for $P(\omega)$ (see (9) and Fig. 1) it follows that the instability condition for the fd-SSM can be satisfied only for $N = \pm 1$ or $N = 0$, and this can only occur either for $|\omega| \approx \omega_{\max}$ or for $\omega \approx \Omega_0$, respectively. (This can be confirmed by plotting the entire graph of $\delta(\omega)$, which looks qualitatively similar to the graph of $P(\omega)$ and hence is not shown here.) Later on we will demonstrate that in the the latter case, a NI cannot occur as long as condition (40) is satisfied. Therefore, for now we focus on the former case, i.e. when $|\omega| \approx \omega_{\max}$.

In this case, the argument of arctangent in (9) is a large number (see (38)), which allows one to use Taylor expansion of that function. In that manner, it is possible to obtain asymptotic expressions for δ_{main} and δ_{ali}. However, for finding an instability threshold, it sufficies to obtain the expressions for $\max|\delta_{\text{main}}|$ and $\max|\delta_{\text{ali}}|$, which occur at $\omega_{\max}$ and $-\omega_{\max}+\Omega_0$, respectively. It turns out that up to terms $O((\beta_2 r)^{-2})$, these expressions coincide and are given by:

$$\max|\delta| = \pi - 2/(|\beta_2|r) - 2\text{arctan}\left((\Omega_0/\omega_{\text{thr}})^2/\sqrt{3}\right). \tag{41}$$

Here we have used $\sin^2(\Omega_0\Delta t/2) \approx (\Omega_0\Delta t/2)^2$, based on (40) and (39). Also, the sign of δ coincides with that of β_2. Using this information and condition (20), one concludes that NI can occur only when $\beta_2 > 0$ for $N = 1$, provided that

$$2/(\beta_2 r) + 2\text{arctan}\left((\Omega_0/\omega_{\text{thr}})^2/\sqrt{3}\right) < 2\epsilon. \tag{42}$$

This condition can be satisfied only for a sufficiently small $\Omega_0/\omega_{\text{thr}}$, whereby one can replace the arctangent in (42) by its argument. Then the stability condition of the fd-SSM becomes:

$$\Delta z < \Delta t/\sqrt{\beta_2\gamma A^2 - (\beta_2\Omega_0/2)^2} \tag{43a}$$

for

$$\Omega_0^2 < 4\gamma A^2/\beta_2. \tag{43b}$$

For $\Omega_0 = 0$, (43a) reduces to the stability condition obtained in [13]. When Ω_0 exceeds the bound given by (43b), the fd-SSM on the background of a moving plane wave is unconditionally stable. Note again that (42) and (43) pertain to the case $\beta_2 > 0$. For $\beta_2 < 0$, no NI can occur for any Ω_0, which follows from (20) and (41).

Let us now discuss how the instability condition (20) can be satisfied for $N = 0$. As mentioned earlier, this requires $\omega \approx \Omega_0$, in which case one can Taylor-expand the expression for $P(\omega)$ around $\omega = \Omega_0$. Substituting the result into (20) with $N = 0$, one finds:

$$-2\epsilon < P''(\Omega_0)(\omega - \Omega_0)^2/2 < 0. \tag{44}$$

As long as $P''(\Omega_0)$ is close to its nominal value of $\beta_2\Delta z$, which is guaranteed by condition (40), condition (44) yields the familiar condition for the occurrence of modulational instability, already mentioned in Section 3:

$$0 < (\omega - \Omega_0)^2 < 2\gamma A^2/(-\beta_2), \tag{45}$$

which, of course, is only possible for $\beta_2 < 0$. This is a real physical instability, and not a numerical one. However, when Ω_0 exceeds ω_{thr}, then $P''(\Omega_0)$ and β_2 will have opposite

signs. Then, if one simulates a plane wave (3) with $\Omega_0 > \omega_{\rm thr}$ using the fd-SSM, one will obtain physically meaningless results. In particular, one will *not* have modulational instability for $\beta_2 < 0$, but will have it for $\beta_2 > 0$.

The results of this section suggest that in simulating signals with nonzero frequency by the fd-SSM, the restrictions on the step size Δz must be imposed based not on stability, but on the bounds (39), (40), which have come from numerical accuracy considerations. Indeed, let us suppose that z, t, and u in (1) are normalized so that $|\beta_2| = 1$, $\gamma = 1$, $A = 1$, and let us take $\Delta t = 0.02$ in (7). This discretization then has temporal accuracy of $O(\Delta t^2) \sim 10^{-4}$–$10^{-3}$, which is quite sufficient for most fiber-optical simulations. The stability condition (43a) implies that Δz may be chosen to be about Δt *or even greater, depending on* Ω_0. So, let us take $\Delta z = \Delta t = 0.02$. Then (39) and (40) dictate that Ω_0 not exceed a value of about 5, which is less than 4% of $\omega_{\rm max} = \pi/\Delta t \sim 150$. The only way to increase the allowed Ω_0 is to increase $\omega_{\rm thr}$, which can only be achieved with smaller Δz, where no NI will be observed.

5 Numerical simulations for the s-SSM

Simulations by s- and fd-SSMs of the plane wave (3) perturbed by a small noise confirm all of the above results. However, these results may become of interest to applications only if they shed some light on the instability of the SSM for a signal which, unlike the solution (3) with constant amplitude and phase, carries information. In this section we consider two types of such signals. First, in Section 5A, we will consider a single channel carrying a sequence of pulses with either regularly or randomly arranged phases. The power of these pulses is sufficiently high, so that the characteristic nonlinear and dispersive lengths are of the same order of magnitude. Such a channel is much more nonlinear than those occurring in fiber-optical telecommunications. In fact, the nonlinearity is strong enough to make NI develop *from noise*. Our purpose of considering such a strongly nonlinear system is to find out how the results of the above plane-wave-based analysis change with the signal format.

Second, in Section 5B, we will consider examples of NI occurring in a realistic, multi-channel telecommunication system. Since such a system is weakly nonlinear, NI generated by a single channel and seeded by noise is too weak to produce any noticeable effect. However, if NI is seeded by another channel or FWM tone, its effect becomes observable. While a careful consideration of NI in multi-channel systems requires a separate study, one can still use results of the analysis in this paper to predict when NI may become detrimental, and hence should be avoided, in realistic telecommunication systems.

For the reason explained at the end of Section 4, we will discuss only the s-SSM.

A. Strongly nonlinear single-channel system

We will consider sequences of pulses with discrete phases. Phase-encoded return-to-zero signals have this form, although they have a much smaller power than considered here. The parameters in (1) in our simulations were: $\beta_2 = 1$ or -1, and $\gamma = 1$; the computational domain was $T = 200$, and the number of grid points was 4096. (So many points were needed not for numerical accuracy, but to guarantee that the computational spectrum amply accommodates the signal's spectrum; see a typical example in Fig. 4(b).) As for the input signal, we have considered a sequence of sech-shaped pulses:

$$u(t,0) = e^{i\Omega_0 t} \sum_{j=1}^{N_{\rm pulse}} \mathrm{sech}\left[t + (N_{\rm pulse} + 1 - 2j)T_{\rm bit}/2\right] \times e^{i\,\varphi_j} + \xi(t), \qquad (46)$$

where $N_{\rm pulse}$ is the number of pulses, $T_{\rm bit} = T/N_{\rm pulse}$ is the interpulse separation, and we will comment on the phases φ_j in the next paragraph. Also, $\xi(t)$ is a Gaussian random process with zero mean and the standard deviation of 10^{-3}. As we announced in the preamble, this noise will seed NI. When $\beta_2 = -1$ and $\beta_3 = 0$, each pulse in (46) is a soliton. We ran all the simulations up to $z_{\max} = 40$. For $N_{\rm pulse} > 28$, pulses are less than four full widths apart, which causes significant interpulse interaction; therefore, we used $N_{\rm pulse} \le 28$.

For the phases φ_j in (46), we have considered two models. In the first model, $\varphi_j = j\,\pi/2$. When $\beta_2 = -1$, this choice minimizes the interaction between adjacent solitons, so that the signal profile (46) is almost unchanged at $z = z_{\max}$. For $\beta_2 = 1$, the pulses are not solitons and hence undergo dispersive broadening and interact with each other, but the profile $u(t,z)$ still remains regular (although changing with z). In the second model, $\varphi_j = 2\pi\chi_j/M$, where χ_j is a random integer between 0 and $M-1$. This choice presents a very simple model for a signal format where the information is encoded in M phase levels. We have considered the cases $M = 2$ and $M = 8$. When $\beta_2 = -1$, interaction of some of the neighboring solitons in this model leads to their (quasi)periodic coalescnece and splitting during the propagation. Thus, the signal power profile acquires some randomness (more so for $M = 8$ than for $M = 2$), although most of the solitons still retain their individuality at $z = z_{\max}$. On the other hand, when $\beta_2 = 1$, the spreading non-solitonic pulses create a power profile which at each z appears as random. This distinction between the degree of randomness in the profiles for $\beta_2 = -1$ and $\beta_2 = 1$ will be referenced below.

Our main results in regards to the NI of signal (46) can be summarized as follows. First, we have verified that the frequencies of the NI bands are predicted by expressions (26a) in the main frequency interval (see Figs. 2 and 3) within 2% of $\omega_{\max}$. Locations of the bands vary with the phase model, $N_{\rm pulse}$, and Δz; this is in qualitative agreement with the results of [6] for the NI of a single soliton. Also, different realizations of the seed noise $\xi(t)$ may result in substantially different amplitude of the unstable modes at $z_{\max}$. In the aliased interval, the accuracy of the prediction by (26b) is less, and it decreases as one approaches the tip of a "sideways parabola" in Fig. 3(a) and 3(c). An example is shown in Fig. 4(a) for: $\Omega_0 = \omega_{\max}/3$, $\beta_2 = 1$, $\beta_3 = 0$, and the first phase model with $N_{\rm pulse} = 27$. For the opposite sign of β_2 and for a different signal phase model, the results are qualitatively similar. In regards to the results shown in Fig. 4(a), we note that for some Δz, we did not observe any NI. This possibility was pointed out in [13] and occurs simply because the width of the NI band may be smaller than the grid spacing $\Delta\omega$. Just slightly (by 0.1%) changing Δz brought the instability back [6], and then it was reported in the figure.

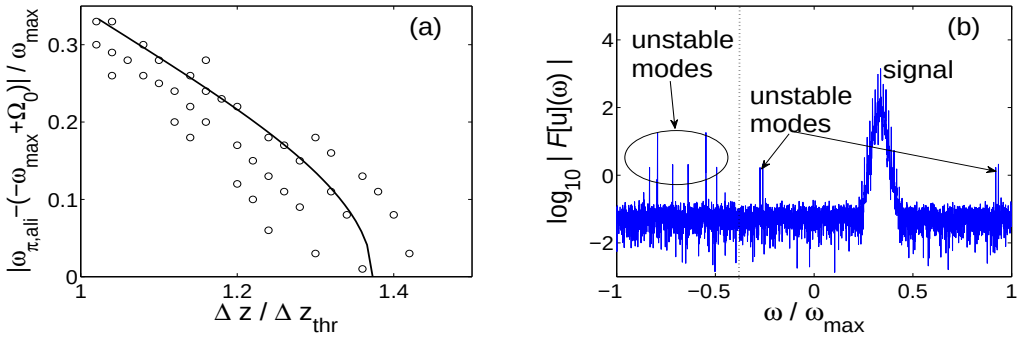

Figure 4: (a) Frequencies of the unstable modes in the aliased frequency interval (see Fig. 2): solid line — computed from (26b); circles — obtained numerically as explained in the text. Several circles for the same value of Δz indicate that for this Δz, multiple isolated unstable modes are observed, as illustrated in the next panel. (b) Spectrum of the numerically computed solution for $\Delta z = 1.25\Delta z_{\rm thr}$, showing multiple unstable modes in the aliased frequency interval. The vertical dashed line separates the aliased and main frequency intervals. **[NOTES FOR PRODUCTION EDITORS: 1) PLEASE PLACE THE FIGURES ONE UNDER THE OTHER (THIS MAY SAVE SOME SPACE). 2) COLOR ONLINE ONLY.]**

Our second main result concerns the growth rate of NI. First of all, it is considerably

lower than the value γA^2 predicted in Section 3. Second, it strongly depends on the temporal profile of the signal. Specifically, the more regular the signal's profile, the stronger the NI. For example, for the first phase model, the unstable modes grow at $z_{\max} = 40$ to be, on average, about an order of magnitude greater for $\beta_2 = -1$ (well separated, almost non-interacting solitons) than for $\beta_2 = 1$ (strongly overlapping pulses, though still preserving a regular pattern). Similarly, for $\beta_2 = -1$, the instability is stronger for the first phase model, where pulses maintain a regular pattern, than for the second one, where pulse phases are random. In particular, the increased phase randomness for $M = 8$ results in the NI being weaker for that case than for $M = 2$. Finally, for $\beta_2 = 1$ and the second (i.e., random) phase model with either $M = 2$ or $M = 8$, where the signal's profile appears as random at $z > 0$, we did not see any substantial growth of numerically unstable modes at $z = 40$ for any Δz up to $\Delta z = 3\Delta z_{\text{thr}}$.

These results about the NI of a spatially-varying solution being considerably weaker than that of a plane wave, are in qualitative agreement with similar results on the background of a single soliton [6]. However, a detailed study of the dependence of the instability growth rate on the signal profile is an open problem.

Finally, we have verified the prediction made in Section 3 that for $\Omega_0 > 0.5\omega_{\max}$, the s-SSM is unconditionally (i.e., for any step size Δz) unstable. For the first phase model, spectral location of the NI bands as functions of $\Omega_0/\omega_{\max}$ (not $\Delta z/\Delta z_{\text{thr}}$; see (30) and a note after it) and the spectrum of the numerical solution look qualitatively similar to those shown in Fig. 4. For $\beta_2 = 1$ and the second phase model, this instability is also too weak to be observed at $z = 40$, but it is observed at longer propagation distances.

B. Weakly nonlinear multi-channel system

As we announced in the preamble to this section, in weakly nonlinear systems, which occur in fiber-optical communications, a NI seeded by noise would be too weak to affect simulation results. However, if the spectral locations of NI bands created by channel X coincide with those of channels Y and Z and/or of FWM tones, then the NI may indeed affect the simulated signal's quality. The following two facts imply that such coincidences may generically occur in simulations of multi-channel systems with uniform channel spacing.

Fact 1: If for some Δz, a NI band created by channel X in the *main* frequency interval "hits" channel Y, then, reciprocally, a main-interval NI band of channel Y hits channel X. This is schematically illustrated in Fig. 5(a) and is easily derived from (28a)

and (24); the corresponding $\Delta z_{(X,Y)}$ is given by:

$$\Delta z_{(X,Y)} = \Delta z_{\mathrm{thr},0}\,(\omega_{\max}/(\Omega_{0,X} - \Omega_{0,Y}))^2, \tag{47}$$

where

$$\Delta z_{\mathrm{thr},0} = 2\pi/(|\beta_2|\omega_{\max}^2) \tag{48}$$

is the threshold for $\Omega_0 = 0$ and $\Omega_{0,\{X,Y\}}$ are the frequencies of channels X, Y. Here and below we have set $|N|$ defined in (20) equal to one; for $|N| \neq 1$ a generalization is straightforward. Note that since the right-hand side of (47) is determined by the frequency separation $|\Omega_{0,X} - \Omega_{0,Y}|$, then the same "connection" that occurs between channels X and Y at $\Delta z = \Delta z_{(X,Y)}$ will also occur between any pair of channels X′ and Y′ as long as $|\Omega_{0,X'} - \Omega_{0,Y'}| = |\Omega_{0,X} - \Omega_{0,Y}|$.

Fact 2: If one of the main-interval NI bands created by channel X hits channel Y, then the other such band hits a FWM tone of these channels; see Fig. 5(a). This follows from (28a).

We carry out simulations for a 10-Gb/s terrestrial dispersion-managed-soliton-based system described in [21, 22]; a full description of simulation parameters is given in [23]. We restrict our attention to the case of path-average dispersion equal to 0.36 ps/nm/km, 50%-duty cycle pulses, and seven 50-GHz spaced channels, located at 150, 100, ..., -150 GHz, with the frequency of channel 1 being 150 GHz. Postcompensation for all channels is set to 0 ps/nm/km, which is at or near optimum. The computational spectrum extends from -320 to 320 GHz. The dispersion in this system alternates sign between the span ($D_{\mathrm{span}} \approx 5.8$ ps/nm/km) and the dispersion-compensating module (DCM; $D_{\mathrm{DCM}} \approx -132$ ps/nm/km). Unless the ratio $\Delta z_{\mathrm{span}}/\Delta z_{\mathrm{DCM}}$ is chosen to equal $|D_{\mathrm{DCM}}/D_{\mathrm{span}}|$ (see (24)), NI in the span and DCM will occur at different frequencies. (Note that path-average dispersion plays no role in setting a NI; it is only the local dispersion that does.) For simplicity, we set Δz_{DCM} below the instability threshold, so that NI may occur only in the span. Thus, in what follows $\Delta z \equiv \Delta z_{\mathrm{span}}$.

To illustrate how NI can affect this system, we chose to vary Δz near a value $\Delta z_{(1,4)}$ (see (47)), where NI created by channel 1 hits channel 4 (at 0 GHz). According to Fact 2 above, the NI will simultaneously hit the FWM tone at 300 GHz. According to Fact 1, similar "interaction" will also exist within pairs (2,5), (3,6), and (4,7) of the channels. Note that the effect of NI is expected to be the strongest for channel 4, because both its NI bands hit channels (1 and 7), whereas one of the NI bands of any other channel will hit a FWM tone, which has a lower power than a channel.

In addition to this NI, there may also occur NI involving modes from the aliased frequency interval. However, in general, there is no guarantee that if one aliased NI

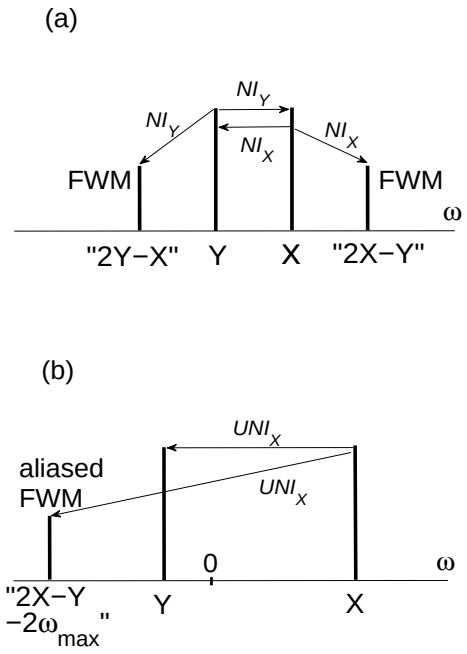

Figure 5: Schematics illustrating Facts 1 – 3. **[NOTE FOR PRODUCTION EDITORS: PLEASE PLACE THE FIGURES ONE UNDER THE OTHER (THIS MAY SAVE SOME SPACE).]**

band hits a channel then the other band will hit another channel or a FWM tone, and the situation must be examined on a case-by-case basis by analyzing plots like the one in Fig. 3(a). For the case at hand, (28b) predicts that for $\Delta z \approx 1.09\Delta z_{(1,4)}$, the inner band of aliased NI hits channel 5 (at -50 GHz). The outer band is then at -290 GHz, which is close to the FWM tone at -300 GHz. Thus, an aliased NI can develop at this or nearby value of Δz.

To verify the above predictions, we varied Δz in the interval $[0.90\Delta z_{(1,4)} \ldots 1.26\Delta z_{(1,4)}]$ and recorded the eye closure (EC) of the channels. For each Δz, we ran simulations for ten different interchannel bit delays. The EC values we report below are the average ones over these ten simulations. In Fig. 6 we plot the results as $\max(\mathrm{EC}_1, \mathrm{EC}_7)$, $\max(\mathrm{EC}_2, \mathrm{EC}_6)$, $\max(\mathrm{EC}_3, \mathrm{EC}_5)$, EC_4, where the subscript denotes the channel's number. The channels are paired up according to their symmetry relative to $\omega = 0$; the maximum EC is a relevant metric of system performance. As a benchmark, we also measured ECs for $\Delta z < \Delta z_{\mathrm{thr},\,0}$, and they are practically the same as those for $\Delta z = 0.9\Delta z_{(1,4)}$.

We will now discuss the main points conveyed by Fig. 6.

Near $\Delta z = \Delta z_{(1,4)}$, NI causes a substantial increase of EC of all channels. This is consistent with Fact 1, whereby all channel pairs with $|\Omega_{0,X} - \Omega_{0,Y}| = 2\pi|150 - 0|$ GHz are affected. Channels 1, 4, 7 are affected the most, as we have explained three paragraphs above. The other substantial increase of EC occurs near $\Delta z = 1.18\Delta z_{(1,4)}$, with the affected channel pairs being (1,5) and (3,7). We believe that if the reason behind this spike of EC is the single-channel-generated NI studied in this work, then it must be the NI with $|N| = 2$ in Eqs. (20) and (26a). Indeed, using (46), one has $1.18\Delta z_{(1,4)} = 2.1\Delta z_{(1,5)} \approx 2\Delta z_{(1,5)}$. Other supporting evidence for this conclusion came from our extensive experimentation with removing (i.e., filtering out) various combinations of channels and/or FWM tones as well as by increasing the width of the spectral domain so as to avoid aliased NI. Although this has led us to believe that the origin of the spike at $\Delta z = 1.18\Delta z_{(1,4)}$ is as stated above, we point out two issues about it which at the moment remain not understood. First, it is unclear why the spike did not occur at $1.12\Delta z_{(1,4)}$, which value equals $2\Delta z_{(1,5)}$ almost exactly rather than within 5%. Second, we verified that if one keeps only channels 1, 3, 5, 7, the spike in EC is almost the same as with all the channels being present. However, removing any one channel from that group (e.g., keeping only 1, 3, and 5) eliminates the spike completely. This is strange, because channels 1 and 5 should still interact via NI, whereas channels 3 and 7 seem to have no effect on that interaction. These open issues may only be resolved after one analyzes the possibility that this spike is due to a NI generated by more than one channel, which we did not study here.

We also note that near $\Delta z = 1.09\Delta z_{(1,4)}$, where, according to (28b), one can expect an aliased NI band created by channel 1 to hit channel 5 and the FWM tone near -300 GHz, we see *no* significant change in EC values. The reason for that is unclear. Nevertheless, one can conclude from this and previous observations (see the data in Fig. 6 for channels 2, 3, 5, 6 at $\Delta z = \Delta z_{(1,4)}$) that when a NI hits a channel and a FWM tone, that affects the simulated signal's quality much less than when it hits two channels.

Reasoning along the same lines, one may expect that when a NI hits two FWM tones, it is even weaker than when it hits a FWM tone and a channel. To verify that, we considered situations where the main-interval NI bands of channel 4 (at 0 GHz) hit FWM tones at ±200, ±250, or ±300 GHz. The corresponding values of Δz are found from (47) to be: $2.56\Delta z_{\mathrm{thr},0} \equiv \Delta z_{(1,5)}$, $1.64\Delta z_{\mathrm{thr},0} \equiv \Delta z_{(1,6)}$, and $1.14\Delta z_{\mathrm{thr},0} \equiv \Delta z_{(1,7)}$. We have observed almost no variation (no more than 0.01 dB) in any channel's EC when Δz was varied near the latter two values. When it was varied within 10% of the first

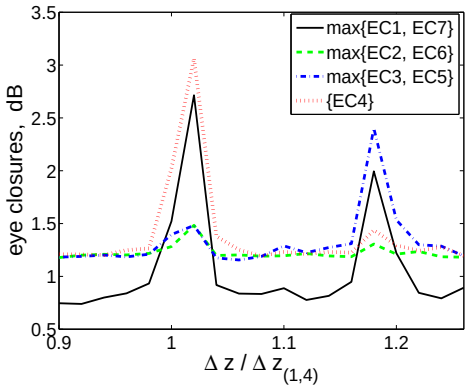

Figure 6: Simulated signal quality versus Δz. **[NOTE FOR PRODUCTION EDITORS: COLOR ONLINE ONLY.]**

value, the EC of channel 4 was almost not affected, while the ECs of all other channels fluctuated by up to 0.2 dB. This is consistent with the observation made in the previous paragraph about the effect of a NI that hits a channel and a FWM tone; note that in this case, e.g., the NI created by channel 2 hits channel 6 and the FWM tone at 300 GHz, etc.

Thus, if a NI hits two FWM tones, it does not affect the quality of the simulated signal, and when it hits a channel and a FWM tone, it affects the signal quality by only a small fraction of a dB. Therefore, in simulation of realistic transmission systems, Δz may be taken so large that the NI of the most numerically unstable (i.e., central) channel hits frequencies between an edge channel and the first FWM tone, and this should not considerably affect simulation results. Quantitatively, this yields:

$$\Delta z \approx \Delta z_{\mathrm{thr},\,0}\left(\omega_{\max}/(\Omega_{0,\,\mathrm{edge}} + 0.5\Delta_{\mathrm{ch}}\Omega)\right)^2, \tag{49a}$$

where $\Omega_{0,\,\mathrm{edge}}$ is the frequency of the edge channel and $\Delta_{\mathrm{ch}}\Omega$ is the interchannel spacing. Alternatively, one can use

$$\Delta z \leq \Delta z_{\mathrm{thr},\,0}\left(\omega_{\max}/(\Omega_{0,\,\mathrm{edge}} + 1.5\Delta_{\mathrm{ch}}\Omega)\right)^2, \tag{49b}$$

which guarantees that NI will occur sufficiently beyond the first FWM tone and hence will not affect the signal.

To conclude this section, we will investigate whether the unconditional (i.e., independent of Δz) NI (UNI) which occurs when $\Omega_0 > 0.5\omega_{\max}$ could be strong enough to affect simulations of realistic transmission systems. Before proceeding, we state the following.

Fact 3: If the inner (i.e. closer to $\omega = 0$) UNI band created by channel X hits channel Y, then the other band hits the *aliased* FWM tone of these channels. This is illustrated in Fig. 5(b) and follows from (30) and the expression for the frequency of the aliased FWM tone: $\omega = 2\Omega_{0,X} - \Omega_{0,Y} - 2\omega_{\max}$. Thus, such a UNI will involve two channels and one (aliased) FWM tone.

First, we performed a proof-of-principle simulation where we shifted all seven channels towards positive ω by the same amount while keeping $\Delta_{\text{ch}}\Omega$ fixed. We indeed observed that when the UNI of channel 1 hit either channel 7 or 6 (according to formula (30)), the EC of channel 1 increased by more than 1 dB and by 0.3 dB, respectively. Somewhat surprisingly, EC_7 and EC_6 were not noticeably affected.

However, a setup described in the previous paragraph does not typically occur in simulations. A more practical situation is where the spectrum is symmetric with respect to $\omega = 0$, but $\Delta_{\text{ch}}\Omega$ may be chosen so that $\Omega_{0,\,\text{edge}} > 0.5\omega_{\max}$. In Fig. 7 we report the corresponding results where we have varied $\Delta_{\text{ch}}\Omega/(2\pi)$ between 50 and 56 GHz. The condition $\Omega_{0,\,\text{edge}} = 0.5\omega_{\max}$ occurs for $\Delta_{\text{ch}}\Omega/(2\pi) = 53.7$ GHz, whereas the UNI of channel 1 hits channel 6 (according to formula (30)) for $\Delta_{\text{ch}}\Omega/(2\pi) = 54.5$ GHz; the same applies to the channel pair (7,2). (The location of the UNI bands changes very rapidly with $\Delta_{\text{ch}}\Omega$ due to the square-root dependence in (30).) Let us emphasize that the strong increase of the EC of the edge channels seen in Fig. 7 is caused *not* by the UNI but rather by the perfectly phase-matched aliased FWM between channels 1 and 7. A sign of the UNI is only a modest increase of the EC of channels 2 and 6. Let us also note that another modest increase in EC observed near $\Delta_{\text{ch}}\Omega/(2\pi) = 58$ GHz may be attributed both to the UNI of channel 1 (7) hitting channel 5 (3) and to the aliased FWM tones of channels 1 and 7 hitting channels 2 and 6. Thus, we conclude that while the UNI does indeed affect the simulated signal quality, such an effect may be masked by a possibly stronger effect of aliased FWM.

6 Conclusions

We have studied the occurrence of NI in the popular split-step method (SSM), which is commonly used to simulate the nonlinear Schrödinger equation. We considered both the spectral and a finite-difference version of the SSM. Analysis was done for a single plane wave (3) with a nonzero frequency Ω_0. Simulations were carried out not only for this solution, but — for the s-SSM — also for a single channel propagating multiple pulses with different phase modulation profiles, as well as for a realistic multi-channel communication system. Below we compare results of the analysis and simulations for

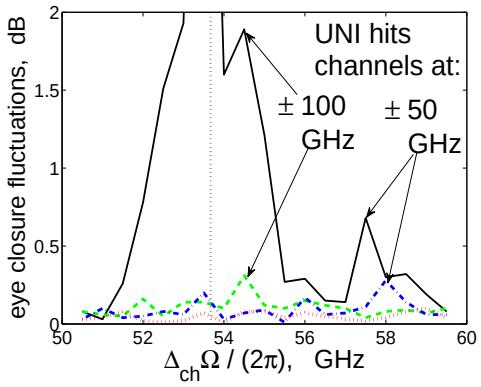

Figure 7: Fluctuations of simulated signal quality, defined as $\max|\mathrm{EC}_{4\pm n} - \mathrm{EC}_{4\pm n,\,\mathrm{benchmark}}|$, where $n = 0, \ldots, 3$ and $\mathrm{EC}_{k,\,\mathrm{benchmark}}$ is measured for $\omega_{\max}/(2\pi) = 640$ GHz and $\Delta z < \Delta z_{\mathrm{thr},\,0}$ to avoid aliasing and NI. Colors and line styles correspond to the same channels as in Fig. 6. The vertical line marks where $\Omega_{0,\,\mathrm{edge}} = 0.5\omega_{\max}$. The fluctuation outside the vertical limits of the figure is approximately 6 dB. **[NOTE FOR PRODUCTION EDITORS: COLOR ONLINE ONLY.]**

the s-SSM and at the end state conclusions for the fd-SSM.

First, analytical formulae for the step size's threshold, (27a) or (36a), and spectral locations of the NI bands in the main frequency interval, (26a) or (35a), turn out to be accurate for a realistic, multi-pulse, signal. Note that having $\Omega_0 \neq 0$ raises the NI threshold compared to the case $\Omega_0 = 0$. The NI threshold and bands' locations are only slightly affected by the nonlinearity, and hence the presence of loss and gain, in the system; see the sentence after (28). On the other hand, in the aliased frequency intervals, NI of a multi-pulse signal may occur at locations different from those predicted by the plane-wave-based analysis; a typical situation is shown in Fig. 4. This difference is small near the wide part of the parabola, but increases towards its tip.

Second, growth rate of NI is considerably smaller for a multi-pulse signal than for a plane wave. This, perhaps, has been known before, but not widely quoted; the only reference known to us where a related result for a single soliton was stated is our own work [6]. Moreover, NI is much stronger on the background of a signal that preserves (or regularly changes) its shape during the propagation rather than a signal that changes shape (pseudo) randomly. Practically important examples of the latter kind of signal are highly dispersed pulses, which are used in modern transmission systems, especially

after the advent of electronic dispersion compensation. A theoretical explanation of the dependence of the NI growth rate on the shape of the signal remains an open problem.

Third, a NI created by a channel in a realistic multi-channel transmission systems is too weak to affect the signal unless at least one NI band hits another channel and the other band hits either a channel or a FWM tone. This situation may generically occur with NI bands in the main frequency interval, as defined in Section 3. The NI in the aliased interval may only hit a channel and a FWM tone, and such an occurrence can be analyzed on a case-by-case basis using a plot as in Fig. 3(a). We have also shown that while a NI hitting two channels dramatically (by more than 1 dB) affects the eye closure of an on-off-keyed signal, its effect is much weaker (0.3 dB or less) if it hits a channel and a FWM tone. Based on our numerical experiments, we have concluded that NI will not cause a noticeable effect to the simulated signal as long as the integration step is chosen according to (49). Note that this value is considerably greater than the threshold $\Delta z_{\mathrm{thr},\,0}$, which would apply to the NI developing from noise (as opposed to a channel). Consequently, using Δz given by (49a) instead of $\Delta z < \Delta z_{\mathrm{thr},\,0}$ reduces the simulation time by a factor between 3 and 4 without affecting the simulation results.

Let us also note that in simulations of transmission systems employing pseudo-randomly varying signals mentioned two paragraphs above, NI may be even weaker than we reported in Section 5B, where the pulses were dispersion-managed solitons and hence had a regularly varying profile. Whether this observation may allow one to relax condition (49) when simulating pseudo-randomly varying signals, is an open problem.

Fourth, we have shown, for the first time to our knowledge, that the s-SSM can be stable only when $\Omega_0 < 0.5\omega_{\max}$. If this condition is violated, a NI will develop for any step size Δz. Two remarks are in order here. On one hand, from the formal point of view, the mechanism of this unconditional NI is different from that behind aliased FWM which leads to exactly the same condition, $\Omega_0 < 0.5\omega_{\max}$ [19]. Indeed, in [19], the coefficient '0.5' occurred specifically for the cubic nonlinearity in (1); for a different type of nonlinearity (e.g., quadratic [20] or quintic), it would have been different. In contrast, our condition (25) was obtained based solely on the form of the dispersion term and the nonlinearity being of the form $F(|u|)u$, with an arbitrary function F. This can be easily verified by replacing the nonlinear term in (1) by, say, $|u|^4u$ and repeating the calculations of Section 2. Then, upon neglecting terms $O(\gamma|u|^4\Delta z) \ll 1$, one will again arrive at (25) and (30). We provide additional mathematical details in Appendix A. On the other hand, from a practical standpoint, for realistic multi-channel communication systems, this unconditional NI may be masked by an aliased FWM between channels, and hence distinguishing between these two numerical artifacts may become an issue

of academic interest only. We believe that condition (25) may be violated without a noticeable effect on the simulated signal quality, as long as one verifies that neither aliased FWM nor UNI hits channels on the opposite side of the spectrum; condition (49) on the integration step should, of course, still be satisfied.

Even though we have demonstrated by example that our single-channel results could be used to predict occurrences of NI in multi-channel simulations, we emphasize that complete analytical understanding of NI in simulations of multi-channel systems requires at least two more steps. First, for a single chanel, one needs to determine how the signal profile affects the NI growth rate and possibly its spectral locations. Second, one needs to study a NI generated by *two*, and also perhaps three, channels. (Note that in Section 5B we considered a different situation, where NI generated by a single channel hit another one.) Each of these steps requires a separate detailed study.

Finally, for the fd-SSM (2), (7), we have shown (see the end of Section 4) that in a realistic simulation of a signal with a nonzero Ω_0, a limitation on the step size Δz, (40), is imposed by the condition not of numerical stability, but of accurate representation of the evolution of the signal's Fourier harmonics by (7). For more accurate finite-difference approximations of the dispersive step in (2), considered, e.g., in [11], condition (40) will no longer apply, as long as the corresponding $P(\omega)$ accurately approximates (5) over most of the simulated spectrum (see Fig. 1(a,b) in [11]). However, in this case, a stability condition will be similar to that for the s-SSM, because such a condition is determined only by $P(\omega)$; see (19) and (20).

Appendix A: Difference between NI and aliased wave interaction

We demonstrate this difference using the quintic nonlinearity, $|u|^4u$, as an example. It leads to interaction among six Fourier harmonics ("waves") whose frequencies satisfy:

$$\omega_1 + \omega_2 + \omega_3 - \omega_4 - \omega_5 = \omega_6. \tag{A1}$$

Since the interaction among four waves enabled by cubic nonlinearity is called FWM, we will refer to the six-wave interaction as six-wave mixing, SWM. In accordance with our note at the end of Section 2, we imply that SWM requires only condition (A1) but does *not* rely on perfect phase matching among these waves (i.e., it may or may not occur).

In order to observe aliased SWM, one must have $\omega_6 > \omega_{\max}$. This may be possible if the signal has both positive and negative frequencies, e.g., $\Omega_1 = \omega_{\max}/3$ and $\Omega_2 = -\Omega_1$:

$$\Omega_1 + \Omega_1 + \Omega_1 - \Omega_2 - \Omega_2 = (5/3)\omega_{\max} \equiv \Omega_2. \tag{A2}$$

However, it is impossible to have aliased SWM if the signal has only one frequency, which is the situation we analyzed in this work.

Note that if the second frequency component of u is supplied by noise, then the efficiency of SWM is greatly reduced. Indeed, let u_1 be the signal at Ω_1 and u_2 be the noise at Ω_2. Then the wave they create via interaction (A2) is proportional to

$$u_1^3 u_2^{*\,2}, \tag{A3}$$

i.e., its amplitude scales *quadratically* with the noise amplitude. In contrast, the NI process in this case will involve the interactions

$$\Omega_1 + \Omega_1 + \Omega_1 - \Omega_1 - \Omega_2 \qquad \text{and} \qquad \Omega_2 + \Omega_1 + \Omega_1 - \Omega_1 - \Omega_1, \tag{A4}$$

whose corresponding terms,

$$u_1^2 |u_1|^2 u_2^* \qquad \text{and} \qquad |u_1|^4 u_2, \tag{A5}$$

scale *linearly* with the noise amplitude. For a typical noise being 30 dB below the signal, this yields a difference by a factor of 10^3 between (A5) and (A3). Also, from the formal lines of the stability analysis, the latter involves linearization of the equation of motion, where terms (A5) are retained but (A3) are neglected.

Acknowledgement

This work was supported in part by the NSF grants ECCS-0925706 and DMS-1217006. I thank two anonymous referees whose constructive criticism has helped to improve this work.

References

[1] G.P. Agrawal, *Nonlinear fiber optics*, 3rd Ed. (Academic Press, 2001).

[2] G. Strang, "On the construction and comparison of difference schemes," SIAM J. Numer. Anal. **5**, 506–517 (1968).

[3] M. Glassner, D. Yevick, and B. Hermansson, "High-order generalized propagation techniques," J. Opt. Soc. Am. B **8**, 413–415 (1991).

[4] A.A. Rieznik, T. Tolisano, F.A. Callegari, D.F. Grosz, and H.L. Fragnito, "Uncertainty relation for the optimization of optical-fiber transmission systems simulations," Opt. Express **13**, 3822–3834 (2005).

[5] Q. Zhang and M.I. Hayee, "Symmetrized split-step Fourier scheme to control global simulation accuracy in fiber-optic communication systems," J. Lightw. Technol. **26**, 302–316 (2008).

[6] T.I. Lakoba, "Instability analysis of the split-step Fourier method on the background of a soliton of the nonlinear Schrödinger equation," Num. Meth. Part. Diff. Eqs. **28**, 641–669 (2012).

[7] T.I. Lakoba, "Instability of the finite-difference split-step method on the background of a soliton of the nonlinear Schrödinger equation," http://arxiv.org/abs/1208.0578v1 .

[8] G. Bosco, A. Carena, V. Curri, R. Gaudino, P. Poggiolini, and S. Benedetto, "Suppression of spurious tones induced by the split-step method in fiber systems simulations," IEEE Photon. Technol. Lett. **12**, 489–491 (2000).

[9] G. Li, "Recent advances in coherent optical communication," Adv. Opt. Photon. **1**, 279–307 (2009).

[10] X. Li, X. Chen, and M. Qasmi, "A broad-band digital filtering approach for time-domain simulation of pulse propagation in optical fiber," J. Lightw. Technol. **23**, 864–875 (2005).

[11] T. Kremp, "Split-step quasi-spectral finite difference method for nonlinear optical pulse propagation," in *Optical Fiber Communication Conference*, OSA Technical Digest Series (Optical Society of America, 2006), paper OWI8..

[12] P.G. Kevrekidis, *The discrete nonlinear Schrödinger equation: Mathematical analysis, numerical computations and physical perspectives* (Springer, 2009).

[13] J.A.C. Weideman and B.M. Herbst, "Split-step methods for the solution of the nonlinear Schrödinger equation," SIAM J. Numer. Anal. **23**, 485–507 (1986).

[14] F. Matera, A. Mecozzi, M. Romagnoli, and M. Settembre, "Sideband instability induced by periodic power variation in long-distance fiber links," Opt. Lett. **18**, 1499–1501 (1993).

[15] S.A. Chin, "Higher-order splitting algorithms for solving the nonlinear Schrödinger equation and their instabilities," Phys. Rev. A **76**, 056708 (2007).

[16] E. Faou, L. Gauckler, and C. Lubich, "Plane wave stability of the split-step Fourier method for the nonlinear Schrödinger equation," http://arxiv.org/abs/1306.0656v1.

[17] B. Cano and A. Gonzalez-Pachon, "Plane waves numerical stability of some explicit exponential methods for cubic Schrödinger equation," preprint: Appl. Math. Report 2013/1, Univ. Valladolid.

[18] M.H. Holmes, *Introduction to perturbation methods* (Springer, 1995); Sec. 1.5.

[19] S. Derevyanko, "The $(n+1)/2$ rule for dealiasing in the split-step Fourier methods for n-wave interactions," IEEE Photon. Technol. Lett. **20**, 1929–1931 (2008).

[20] J.P. Boyd, *Chebyshev and Fourier spectral methods*, 2nd Ed. (Dover, 2001); Sec. 11.5.

[21] D.F. Grosz, A. Agarwal, S. Banerjee, D.N. Maywar, and A.P.Küng, "All-Raman ultra-long-haul single wideband DWDM transmission systems with OADM capability," J. Lightw. Technol. **22**, 423–432 (2004).

[22] D.A. Fishman, W.A. Thompson, and L. Vallone, "LambdaXtreme® transport system: R&D of a high capacity system for low cost, ultra long haul DWDM transport," Bell Labs Techn. J. **11**, 27–53 (2006).

[23] T.I. Lakoba, "Transmission improvement in ultralong dispersion-managed soliton WDM systems by using pulses with different widths," J. Lightw. Technol. **23**, 2647–2653 (2005).